The Fe–O coordination in iron phosphate glasses by x-ray diffraction with high energy photons



2003 J. Phys.: Condens. Matter 15 6143

(http://iopscience.iop.org/0953-8984/15/36/305)

INSTITUTE OF PHYSICS PUBLISHING JOURNAL OF PHYSICS: CONDENSED MATTER

J. Phys.: Condens. Matter **15** (2003) 6143–6153 PII: S0953-8984(03)65474-3

# The Fe–O coordination in iron phosphate glasses by x-ray diffraction with high energy photons

**U Hoppe[1], M Karabulut[2,3], E Metwalli[2,4], R K Brow[2] and P Jóvári[5]**

[1] Department of Physics, Rostock University, D-18051 Rostock, Germany
[2] Graduate Center for Materials Research, University of Missouri-Rolla, MO 65401, USA
[3] Department of Physics, University of Kafkas, 36100 Kars, Turkey
[4] Glass Research Department, National Research Centre, Dokki, Cairo 12622, Egypt
[5] Hamburger Synchrotronstrahlungslabor (HASYLAB) am Deutschen Elektronen-Synchrotron (DESY), Notkestraße 85, D-22607 Hamburg, Germany

Received 1 July 2003
Published 29 August 2003
Online at stacks.iop.org/JPhysCM/15/6143

**Abstract**

Structures of $(FeO)_x(P_2O_5)_{1-x}$ glasses with $0.2 \leqslant x \leqslant 0.5$ are studied by x-ray diffraction using high energy photons from a synchrotron. Scattering intensities are obtained up to $Q_{max}$ of 250 $nm^{-1}$. P–O, Fe–O and O–O first-neighbour peaks are well resolved in the pair distribution functions. Constant P–O coordination numbers of $4.0 \pm 0.1$ with distances of $0.155 \pm 0.001$ nm are found as expected for $PO_4$ tetrahedra. Mean Fe(II)–O coordination numbers of ∼5 with distances of ∼0.210 nm are extracted from fitting the Fe–O peaks where the oxygen coordination number of the minor fraction of 5–18% Fe(III) was set to six with Fe–O distances of 0.200 nm. The existence of $FeO_5$ or strongly distorted $FeO_6$ polyhedra instead of densely packed $FeO_6$ octahedra for the Fe(II) sites is attributed to the mixed oxide effect. $Fe^{3+}$ cations in rigid $FeO_6$ octahedra hinder the $Fe^{2+}$ cations in forming well defined octahedral environments.

## 1. Introduction

Phosphate glasses containing fractions of iron oxide have been found to possess excellent chemical durabilities, so making them candidates for use in vitrification of high level nuclear wastes [1, 2]. In the corresponding applications multicomponent glasses of the polyphosphate range are used. Most earlier structural studies of Fe phosphate glasses were made on samples of these compositions [3–10], among them binary $(Fe_zO)_x(P_2O_5)_{1-x}$ glasses [8–10]. Possible numbers $z$ range from 0.66 to 1, indicating that iron atoms exist as mixtures of Fe(III) and Fe(II) states. In the polyphosphate range, with $n(O)/n(P) > 3$, a significant fraction (>75 at.%) of iron atoms exists in the Fe(III) state. Their fraction also depends on raw materials and melting conditions [8, 10]. Various Fe–O coordination environments are found by different methods at different glass compositions: four- to five-coordinated sites by Fe–K EXAFS

  

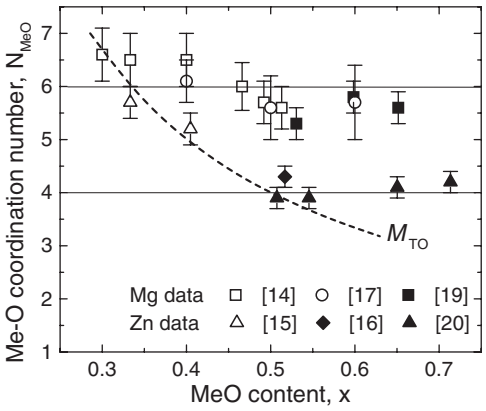


**Figure 1.** Me–O coordination numbers of Zn and Mg phosphate glasses versus MeO content. $M_{TO}$ is the ratio of available terminal oxygen per Me atom.

measurements [10], Fe(III)$O_6$ octahedra and distorted Fe(II)$O_6$ octahedra by Mößbauer spectroscopy [7, 8] and octahedra by Fe–K EXAFS [5] and x-ray diffraction (XRD) [6]. The high durability of such glasses is attributed to rigid octahedral Fe(III) sites which link the short phosphate chains and block migration of other cations [5, 6].

The present XRD work is aimed at studying structural effects of the binary Fe phosphate system in the ultraphosphate compositional range ($n(O)/n(P) < 3$), where an excess of the $P_2O_5$ fraction exists. Structures of such phosphate glasses are known as three-dimensional networks of corner-linked $PO_4$ tetrahedra where three-connected branching units ($Q^3$) coexist with two-connected middle units ($Q^2$) [7, 11]. If glassy samples of high $P_2O_5$ fractions are prepared the corresponding samples have to be molten in sealed ampoules to avoid loss of the volatile $P_2O_5$ fraction and contamination with humidity [12]. Here, FeO is used as starting ingredient and, thus, the majority of iron atoms is expected to be in the Fe(II) state. The four glass samples used in this study are part of a larger series which has already been investigated by Mößbauer and IR spectroscopy [13]. The Mößbauer experiments indicate that 5–18% of the Fe ions are Fe(III) ions and the remainder are Fe(II) ions. Both species are present in octahedral coordination sites [13].

Oxygen environments of Zn ions in binary Zn ultraphosphate glasses ($Zn^{2+}$ ions have dimensions similar to those of $Fe^{2+}$ ions) have been found to change from octahedral to tetrahedral geometry with ZnO fractions increasing from $x = 0.33$ to 0.5 [14–16]. A similar behaviour exists for MgO but only some of the Mg sites change to tetrahedral environments at metaphosphate composition ($x = 0.5$ or $n(O)/n(P) = 3$) [14, 17, 18]. If for $x$ changing from 0.33 to 0.5 the metal–oxygen coordination number, $N_{MeO}$, decreases from six to four, then $N_{MeO}$ changes in agreement with the ratio $M_{TO}$ of available terminal oxygen atoms ($O_T$) per Me. (Bridging oxygen atoms are called $O_B$.) The number $M_{TO}$ decreases upon MeO addition with $M_{TO} = n(O_T)/n(Me) = \nu/x$ [14, 19] where $\nu$ is the valency of Me. Figure 1 shows a comparison of the behaviour of $M_{TO}$ for $\nu = 2$ with experimental numbers $N_{ZnO}$ and $N_{MgO}$.

The effect of $M_{TO}$ on $N_{MeO}$ is explained as follows [19, 21]: all $O_T$ including those of the $PO_4$ branching units are available to coordinate Me atoms. With small MeO fractions ($M_{TO} > N_{MeO}$)$MeO_n$ polyhedra with greater $N_{MeO}$ values are preferably formed isolated from each other, e.g., $ZnO_6$ octahedra in the case of $Zn^{2+}$. The $O_T$ link neighbouring P- and Zn-centred oxygen polyhedra through Zn–$O_T$–P bonds. Thus, the octahedral symmetry extends even to the second coordination shell of the Zn sites. In the transition from $M_{TO} \geqslant N_{ZnO}$

**Table 1.** Compositions of the binary $(Fe_zO)_x(P_2O_5)_{1-x}$ samples studied. Value $z$ is equal to unity in the nominal compositions. According to the Fe(III) fractions detected by Mößbauer spectroscopy [13] the nominal compositions are changed to new $x$ with fixed $n(\mathrm{Fe})/n(\mathrm{P})$ ratio by adding appropriate amounts of oxygen.

| Sample label | Nominal $x$ | $n(\mathrm{FeIII})/[n(\mathrm{Fe})]$ | $z$ value | New $x$ | $n(\mathrm{O})/n(\mathrm{P})$ |
|---|---|---|---|---|---|
| FP2 | 0.20 | 0.18 | 0.940 | 0.21 | 2.64 |
| FP3 | 0.30 | 0.12 | 0.960 | 0.31 | 2.73 |
| FP4 | 0.40 | 0.05 | 0.983 | 0.41 | 2.84 |
| FP5 | 0.50 | 0.06 | 0.980 | 0.51 | 3.02 |

to $M_{\mathrm{TO}} < N_{\mathrm{ZnO}}$ with ZnO additions $N_{\mathrm{ZnO}}$ decreases and maintains Zn–$O_T$–P linkages until only $ZnO_4$ tetrahedra exist. If $M_{\mathrm{TO}}$ becomes less than four the Zn share $O_T$s to fulfil their coordination requirements. Effects of decreasing $N_{\mathrm{MeO}}$ are not only found for Zn and Mg but are also reported for three-valent modifier oxides $Me_2O_3$ with Me = La [21]; Nd, Er [22]; Al [23] and Ga [24]. In the present work, the coordination environments of Fe(II) ions are examined using the structural model described above. The Fe(II) ions differ from the modifiers mentioned above because they possess partially filled d-shells which can cause stabilization effects of definite ligand geometries [25]. Fe–O first-neighbour distances of ∼0.20 nm are similar to those of Zn–O and Mg–O pairs. The Fe–O peaks are expected to be well resolved between the P–O and O–O peaks at ∼0.15 and ∼0.25 nm if XRD with short wavelength synchrotron radiation is used [16–18, 20]. Reliable numbers $N_{\mathrm{FeO}}$ are expected. Neutron diffraction (ND) on spallation sources can reach similar or even greater measuring range with higher resolving power. But such experiments are difficult for iron containing glasses. The magnetic scattering amplitude of the Fe atoms [9, 26] is not properly known.

## 2. Experimental details

The samples are prepared as described in [13]. Raw materials used for melting in sealed silica ampoules are mixtures of $P_2O_5$ (purified by vacuum sublimation) and reagent grade FeO. Melts were held at 1100 °C for 1 h. The ampoules were transferred to a dry box immediately after removing from the furnace. The resulting glasses are black and visibly homogeneous. The batch compositions of the glasses studied are $x = 0.2$, 0.3, 0.4 and 0.5. Mößbauer spectroscopy [13] reveals small fractions of Fe(III) contamination (see table 1). For the analysis of diffraction data such glass compositions are used where the original ratio $n(\mathrm{Fe})/n(\mathrm{P})$ is fixed but the oxygen fraction is increased to take into account the $Fe_2O_3$ fraction. So the actual compositions $x$ are little greater than the nominal ones.

The XRD experiments were performed on the BW5 wiggler beamline at the DORIS III synchrotron (Hamburg) where an energy of incident photons of 115.4 keV ($\lambda = 0.0107$ nm) was used. Glass powders were loaded into 3.0 mm (diameter) silica capillaries with a wall thickness of 0.01 mm. In the scans the detector moves horizontally on a straight line, perpendicularly to the incident beam, in equidistant steps reaching a maximum scattering angle of 25°. Additional runs for reduction of the noise of counting statistics in the high $Q$ range were made for the sample FP5. Since the scattering angles are small the transmission factors are assumed to be independent of the angle. Details of such experiments and the corrections are described elsewhere [27]. The elastic line and the full Compton profile pass the electronic energy window of the solid-state Ge detector. Dead-time corrections are made with values $\tau$ of 1.08 $\mu$s. A fraction of 0.91 of incident photons is polarized horizontally. Corrections are made for background, container scattering, varying sample–detector distance

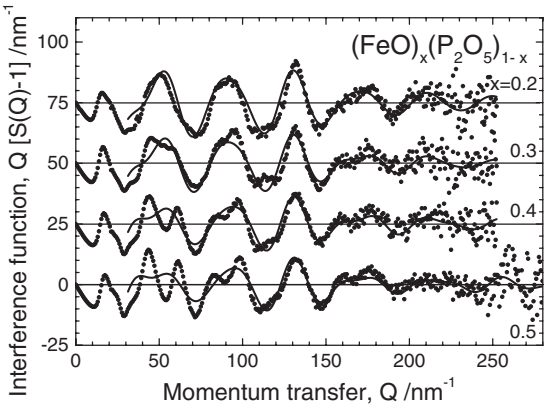


**Figure 2.** Weighted interference functions, $Q[S(Q)-1]$ (dotted curves), of the four iron phosphate glasses studied. The solid-curve functions are calculated using parameters from fitting the P–O, Fe–O and O–O first-neighbour peaks.

and absorption. Scattering intensities are normalized to the structure-independent scattering functions which are calculated by a polynomial approach [28] of tabulated atomic parameters of the elastic scattering factors [29]. Finally, the Compton fractions taken from tabulated data [30] are subtracted and Faber–Ziman structure factors, $S(Q)$, are calculated [31, 32].

## 3. Results

The resulting scattering intensities are plotted in figure 2 by means of the weighted interference functions, $Q[S(Q)-1]$. The experimental functions are compared with model functions which are calculated with parameters of the Gaussian functions fitted to the first-neighbour peaks of P–O, Fe–O and O–O distances (see below). The information in the high $Q$ range is obviously only related to the first-neighbour peaks. The correlation functions, $T(r)$, are calculated by Fourier transformations with

$$T(r) = 4\pi r\rho_0 + 2/\pi \int_0^{Q_{\max}} Q[S(Q) - 1]M(Q)\sin(Qr)\,\mathrm{d}Q \qquad (1)$$

where $\rho_0$ is the number density of atoms. The $\rho_0$ are refined according to the condition $T(r) = 0$ for distances less than the P–O bond length. The values $Q_{\max}$ used are 252 nm$^{-1}$, the upper limit of scattering data, and also 220 nm$^{-1}$. A damping factor $M(Q)$ with $M(Q) = \sin(\pi Q/Q_{\max})/(\pi Q/Q_{\max})$ [33] is used in the case of $Q_{\max} = 252$ nm$^{-1}$ to reduce effects of noise in the high $Q$ range of data. The satellite ripples are clearly damped which makes easier subsequent fitting of peaks. However, damping also causes additional peak broadening. The resulting $T(r)$ functions are given in figures 3(a) and (b). They show a clear decrease of P–O peak intensity and an increase of Fe–O peak intensity with increasing FeO content.

Details of the short range order are obtained by analysing the P–O, Fe–O and O–O first-neighbour peaks by Gaussian fitting. Effects of truncation of Fourier transformation at $Q_{\max}$ (equation (1)) and $Q$-dependence of weighting factors are taken into account as described in [34, 35]. The Marquardt algorithm [36] is used in the fits. Coordination numbers, mean distances and full widths at half maximum (fwhms) are parameters of the model Gaussian functions. The results for the iron phosphate glasses studied are given in table 2.

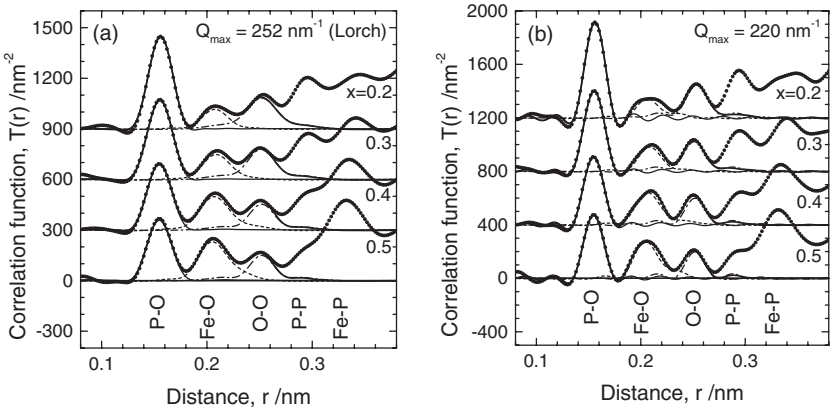


**Figure 3.** Correlation functions, $T(r)$, calculated with different upper limits of measuring range: (a) $Q_{max} = 252\,nm^{-1}$ and Lorch damping [33]; (b) $Q_{max} = 220\,nm^{-1}$. Experimental data—dotted curve; total model function—thick solid curve; P–O peak—thin solid curve; Fe–O peak—dashed curve; O–O peak—dash–dotted curve.

Several assumptions are made in the fits: according to knowledge of different lengths of P–$O_T$ and P–$O_B$ bonds in the $PO_4$ tetrahedra [15, 37, 38] two Gaussian functions are used for fitting the P–O peak. The lengths and frequencies of both bonds change with increasing modifier content. The ratio of their frequencies was calculated from composition $x$ [11, 15] and fixed in the fits. The difference of lengths of the P–$O_T$ and P–$O_B$ bonds was fixed at ∼0.01 nm [15]. The assumption of two Gaussian peaks for the P–O bonds in the fits presented here is not evidential of their existence. But the appearance of split P–O peaks is only a question of resolving power. ND measurements of phosphate glasses with $Q_{max}$ of ∼500 $nm^{-1}$ result in two components of the P–O peak [38].

Fe(III) sites are assumed to be six coordinated in the glasses studied, consistent with the earlier Mößbauer study [13]. The assignment of $N_{FeO} = 6$ for Fe(III) sites is also consistent with the reported octahedral coordination geometries for even smaller $Al^{3+}$ and $Ga^{3+}$ ions in their respective binary metaphosphate glasses [23, 24]. This coordination number is expected to be valid in the ultraphosphate range, as well, where for each Fe(III) introduced three $Q^3$ tetrahedra are changed to three $Q^2$ tetrahedra, now with six $O_T$. The Fe–O distance for this $FeO_6$ octahedron is set at 0.200 nm, consistent with the Fe–O bond distance in $Fe(PO_3)_3$ crystals [39]. Although the Fe–O and O–O peaks are well resolved some parameters of the Gaussian function used for fitting the O–O peak at ∼0.25 nm are fixed. This approach reduces effects from peaks of greater distances such as those of P–P neighbours. Since distance $r_{PO}$ is independent of the modifier content, see table 2, $r_{OO}$ should also be fairly independent of $x$. The O–O edges of the $PO_4$ tetrahedra have lengths of ∼0.252 nm [15, 24]. The numbers $N_{OO}$ are calculated from the ratio of $O_T$ and $O_B$ sites with $N_{OO} = 24/(5 + y)$ [21] where $y$ is $n(MeO)/n(P_2O_5)$ with $y = x/(1 - x)$. An $O_T$ has three and an $O_B$ has six first-neighbour O atoms. Other O–O distances than the tetrahedral edges are greater than 0.27 nm (see the related crystal structures [39–43]). Finally, all other distances between 0.20 and 0.25 nm are attributed to Fe–O correlations of the Fe(II) sites. Two or three Gaussian functions are used in the fits due to an asymmetry of the remaining peak.

At first, fits are made with the $T(r)$ functions shown in figure 3(a) which have been obtained with damping. The resulting parameters are given in table 2 and are used for calculating model functions to compare with the $T(r)$ data shown in figure 3(b). These functions have been

**Table 2.** Parameters resulting from Gaussian fitting of the P–O, Fe–O and O–O first-neighbour peaks. Distances and fwhms are given in nm.

| Sample | Atom pair | Coordination number | Distance | Fwhm | Total coordination number | Mean distance |
|---|---|---|---|---|---|---|
| FP2 | P–O | 1.27[b] | 0.1484[b] | 0.009(2) | 4.0(1) | 0.156(1) |
| | | 2.73[b] | 0.1594[b] | 0.011(2) | | |
| | Fe(III)–O | 6.0[a] | 0.200[a] | 0.020[a] | | |
| | Fe(II)–O | 4.5(4) | 0.208(1) | 0.018(3) | 5.5(6) | 0.210(2) |
| | | 1.0(2) | 0.222(3) | 0.020(4) | | |
| | O–O | 4.55[a] | 0.252[a] | 0.026(4) | | |
| FP3 | P–O | 1.45[b] | 0.1484[b] | 0.011(2) | 4.0(1) | 0.155(1) |
| | | 2.55[b] | 0.1594[b] | 0.013(2) | | |
| | Fe(III)–O | 6.0[a] | 0.200[a] | 0.020[a] | | |
| | Fe(II)–O | 4.0(3) | 0.209(1) | 0.021(3) | 5.0(5) | 0.212(2) |
| | | 1.0(2) | 0.224(3) | 0.025(4) | | |
| | O–O | 4.40[a] | 0.2515[a] | 0.022(4) | | |
| FP4 | P–O | 1.73[b] | 0.1493[b] | 0.009(2) | 4.1(1) | 0.155(1) |
| | | 2.37[b] | 0.1593[b] | 0.012(2) | | |
| | Fe(III)–O | 6.0[a] | 0.200[a] | 0.020[a] | | |
| | Fe(II)–O | 4.0(2) | 0.2065(1) | 0.025(3) | 5.0(4) | 0.212(2) |
| | | 0.7(1) | 0.225(3) | 0.025(4) | | |
| | | 0.3(1) | 0.250(5) | 0.025(5) | | |
| | O–O | 4.22[a] | 0.252[a] | 0.018(4) | | |
| FP5 | P–O | 2.03[b] | 0.1502[b] | 0.009(2) | 4.0(1) | 0.155(1) |
| | | 1.97[b] | 0.1602[b] | 0.012(2) | | |
| | Fe(III)–O | 6.0[a] | 0.200[a] | 0.020[a] | | |
| | Fe(II)–O | 3.6(2) | 0.204(1) | 0.022(3) | 5.0(3) | 0.210(2) |
| | | 1.4(1) | 0.225(3) | 0.026(4) | | |
| | O–O | 3.98[a] | 0.252[a] | 0.016(4) | | |

[a] These values are fixed in the fits.
[b] The ratio of $P–O_T$ and $P–O_B$ bonds is calculated according to the compositions and the difference of $P–O_T$ and $P–O_B$ distances is fixed.

obtained without damping but with smaller $Q_{max}$. Agreement with the experimental data is excellent which confirms the assumptions of the P–O, Fe–O and O–O peaks. An exception is the O–O peak of sample FP2. Here the O–O distance has to be changed to 0.254 nm and, as a consequence, the number $N_{FeO}$ of the Fe(II) sites increases to 6.5. But the small weight of the Fe–O correlations for sample FP2 leads to greater uncertainty of this $N_{FeO}$. Clear differentiation of five- or sixfold coordination of Fe(II) sites is not possible for sample FP2. In the case of sample FP4 a third small component of the Fe(II)–O peak at 0.250 nm is added; for the other samples two Gaussian functions are sufficient to approximate the Fe(II)–O first-neighbour correlations. The third peak component of FP4 is too small to discuss it as specific of this sample.

P–O coordination numbers of four with P–O distances of ∼0.155 nm and O–O distances of ∼0.252 nm indicate the existence of $PO_4$ tetrahedra whose mean bond lengths do not vary with the $Q^3 \rightarrow Q^2$ change upon FeO additions. The mean Fe–O coordination numbers of the Fe(II) sites are also constant with numbers $N_{FeO}$ of ∼5. (A little greater $N_{FeO}$ is found for sample FP2, see above.) The corresponding Fe–O distances are ∼0.210 nm with a flat tail to the right-hand side of the peaks. Further details of the Fe–O distances are not resolved. The two or three broad Gaussians used to fit the Fe–O peak should not be interpreted as separate

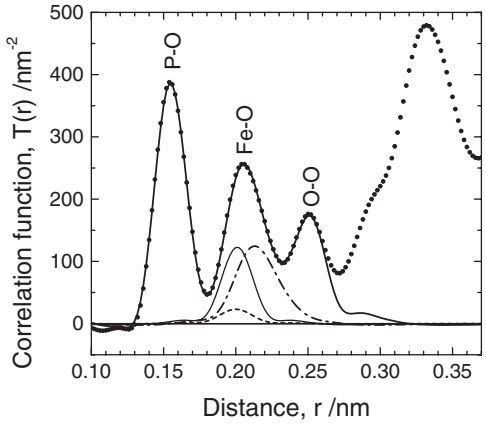


**Figure 4.** $T(r)$ function of the metaphosphate sample FP5 with an Fe(III) fraction of 6%: experimental data—dotted curve; total model function—thick solid curve. The Fe–O peak is split into three components with Fe(III) in octahedral sites—dashed curve, Fe(II) in tetrahedral sites—thin solid curve—and Fe(II) in octahedral sites—dash–dotted curve. Here it is assumed that five-coordinated Fe sites do not exist.

distances. Changes of the conditions of the fits such as small variations of O–O distances or of numbers $N_{\mathrm{FeO}}$ of Fe(III) sites do not change the $N_{\mathrm{FeO}}$ values of the Fe(II) sites much. Possible variations are already included in the uncertainties given in table 2.

Though sufficient reasons exist to assume $N_{\mathrm{Fe(III)O}} = 6$ with $r_{\mathrm{FeO}}$ of ∼0.20 nm (see above) the other case with $N_{\mathrm{Fe(III)O}} = 4$ was checked for sample FP3. The fit leads to $N_{\mathrm{Fe(II)O}} = 5.3$ instead of 5.0 with a decrease of the first Fe(II)–O distance by 0.001 nm. The effect is even smaller for samples FP4 and FP5. Thus, the assumptions for the $Fe^{3+}$ fraction are not critical for determination of parameters of the Fe(II)–O peaks. Additionally, if $Fe^{3+}$ ions form $FeO_4$ tetrahedra then shorter Fe–O distances of 0.185 nm also have to be assumed. The corresponding peak should be found in the minimum between P–O and Fe–O peaks (see figures 3 and 4) where it is not really expected.

P–P and Fe–P peaks at ∼0.295 and ∼0.33 nm are also indicated in figure 3. Fits of these peaks are not performed because of overlap with further pair correlations. Visible changes of the peak heights are mainly due to changes of FeO fractions. In addition, the rupture of P–O–P bridges between the $PO_4$ units with increasing FeO content [11] contributes to the decrease of the peak height of P–P first neighbours.

## 4. Discussion

The main part of the results of the present XRD experiments contributes to the knowledge of oxygen environments of the Fe modifiers in ultraphosphate glasses. The existence of $PO_4$ tetrahedra and of P–O–P bridges confirms other studies [11] of ultraphosphate networks. The general change from the $P_2O_5$ network formed of $Q^3$ units to the chain structure of $Q^2$ units at metaphosphate composition in the samples studied is demonstrated by infrared transmission spectra already reported in [13]. The $Q^3 \rightarrow Q^2$ change depends only on the quantity of oxygen which is introduced with the iron oxide. The existence of mixed Fe(III), Fe(II) states does not affect the fractions of $Q^k$ groups which behave according to the rules of network degradation given by Van Wazer [44].

According to the numbers $N_{\mathrm{ZnO}}$ (or $N_{\mathrm{MgO}}$) found previously [15] and to the model describing this behaviour [19] (see the introduction) the oxygen coordination numbers of the

Fe(II) atoms have been expected to decrease from six to about four for $x$ increasing from 0.33 to 0.5. In these considerations, the effects of the small fraction of six-coordinated Fe(III) sites have been neglected. The values of $N_{FeO}$ are ∼5 and are almost independent of composition. Fe–O coordination numbers of related crystals in the compositional range of glasses studied are six ($FeP_4O_{11}$ [40], $Fe_2P_4O_{12}$ [41]). Thus, the values of $N_{FeO}$ in the glasses differ from those of related ultra- and metaphosphate crystals. Highly distorted $FeO_6$ octahedra ($Fe_2P_2O_7$ [42]) or $FeO_5$ polyhedra ($Fe_3P_2O_8$ [43]) are found in other Fe(II) phosphate crystals.

One model for a glass with $N_{FeO} \sim 5$ is that half of the Fe(II) ions are in tetrahedral sites and half are in octahedral sites. Both coordination environments are stabilized by the ligand fields for $d^6$ ions like $Fe^{2+}$ [25]. Figure 4 shows a deconvolution of the Fe–O peak for sample FP5 based on this model. Contributions to this fit of $Fe^{3+}$ ions are negligible and do not cause significant uncertainties in the determination of the oxygen coordination of $Fe^{2+}$. The fractions of Fe(II) assumed to be in four- and six-coordinated environments would have reasonable Fe–O distances of 0.201 and 0.215 nm, respectively. Both the peaks are broad and there is little prospect of resolving differently coordinated Fe(II) sites by diffraction. The Fe–O distances of the $FeO_6$ octahedra of $FeP_4O_{11}$ [40] or $Fe_2P_4O_{12}$ [41] crystals also form asymmetric peaks but to a lesser extent than those of $FeO_6$ octahedra given in figure 4.

The existence of equal fractions of $FeO_4$ and $FeO_6$ polyhedra for the Fe(II) sites in the phosphate glasses studied would have consequences for the Mößbauer spectra. Indications for the existence of two different Fe(II) sites would be expected. But the spectra are well fitted assuming single Fe(II) sites [13] accompanied by a small signal for the Fe(III) fraction. The Mößbauer hyperfine parameters, isomer shift ($\delta$) and quadrupole splitting ($\Delta$), of the Fe(III) sites (∼0.4 and ∼0.6 mm $s^{-1}$) agree with those of regular $FeO_6$ octahedra (0.42 and 0.51 mm $s^{-1}$ [8]) of the $Fe_3P_4O_{14}$ crystal [45] (room temperature). The parameters $\delta$ and $\Delta$ of the Fe(II) sites (∼1.3 and ∼2.0 mm $s^{-1}$) agree with those of distorted $FeO_6$ octahedra in the $Fe_2P_2O_7$ crystal [42] (1.25 and 2.5 mm $s^{-1}$ [42]) and of $FeO_5$ polyhedra in the $Fe_3P_2O_8$ crystal [43] (1.19 and 2.1 mm $s^{-1}$ [42]). Thus, from findings of Mößbauer spectroscopy [13] and from the mean number $N_{FeO}$ of five found by XRD it is concluded that the majority of Fe(II) atoms is in five-coordinated or strongly distorted six-coordinated oxygen polyhedra. A strongly distorted $FeO_6$ octahedron means that one of the Fe–O distances is greater than 0.26 nm, the upper limit of our Gaussian fits.

As already pointed out above, the $FeO_6$ octahedra of Fe(III) atoms in the glasses studied are all assumed to be formed of $O_T$s from $Q^2$ units where for glasses of $x \leqslant 0.5$ it is not necessary to share these $O_T$s with other Fe atoms. For the Fe(II) atoms regular oxygen polyhedra could also be formed: $FeO_4$ tetrahedra would be possible with the four $O_T$ of the two $Q^2$ groups transformed from $Q^3$ for each Fe(II) introduced. If two $O_T$ from $Q^3$ groups which are available in ultraphosphate structures were involved, octahedra as existing in the $FeP_4O_{11}$ crystal [40] could be formed. Therefore, the $Q^2$ tetrahedra must coordinate the Fe(II) sites by $O_T$–$O_T$ edges only in glasses with low concentrations of Fe(II)O ($x < 0.2$) [19]. The change to more efficient connections of $Q^2$ groups with two Fe sites may explain the increase of $T_g$ beyond its minimum at $x = \sim 0.2$ for this series of Fe ultraphosphate glasses [13].

So far, all Fe atoms could form sites in oxygen polyhedra which do not share corners. If Fe(II) sites form $FeO_6$ octahedra at the metaphosphate composition, they would have to share four $O_T$s with neighbouring Fe(II), as found in the $Fe_2P_4O_{12}$ crystal [41]. From the point of view of the quantity of oxygen available for coordination of the Fe(II) atoms, no reason exists to form $FeO_5$ or distorted $FeO_6$ polyhedra.

Here we remember the effects of iron oxide for the chemical durability [1, 2, 7] if added to phosphate glasses. The effects are valid for binary Fe phosphate glasses as well. Due to the existence of Fe in two oxidation states a mixed oxide effect occurs where $Fe^{2+}$ and $Fe^{3+}$ are the

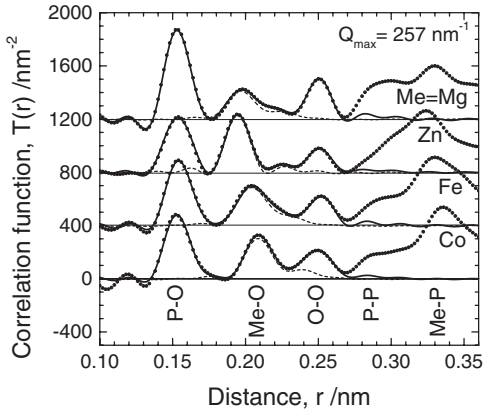


**Figure 5.** Fit of the $T(r)$ functions of Me metaphosphate glasses with Me = Mg, Zn, Fe and Co. Experimental data—dotted curve; total model function—solid curve. The dashed-curve function denotes the Me–O peak which is asymmetric for Me = Mg, Fe and Co. Since the convolution of model peaks with the window function of Fourier transformation is already made some small satellite oscillations occur.

modifier cations of different electric field strengths. From structures obtained by molecular dynamics simulations of K, Na silicate glasses it has been revealed that the geometries of oxygen polyhedra of $Na^+$ cations with stronger field strength are altered at the expense of distortions of those of $K^+$ cations [46]. An analogous effect is assumed for the Fe phosphate glasses: octahedral environments of $Fe^{3+}$ cations surrounded by $Q^2$ groups with short Fe–O distances are fixed in the undercooled melt before regular environments of the $Fe^{2+}$ cations are formed. $Fe(III)O_6$ octahedra possess higher bond energies in mixed glasses than in 'binary' $Fe_2O_3$–$P_2O_5$ glasses. They reduce the ability of $Q^k$ groups to form densely packed oxygen polyhedra for the $Fe^{2+}$ cations. Although the Fe(III) fractions are low (5–18%) in the glasses studied, these quantities appear to be sufficient to cause dramatic effects. Rigid $FeO_6$ octahedra of the Fe(III) sites allow the Fe(II) atoms only to form $FeO_5$ or distorted $FeO_6$ polyhedra. This structural effect is another facet of the high chemical durability of iron-doped multicomponent polyphosphate glasses.

Though the uncertainty of $N_{FeO} \sim 6$ for the Fe(II) sites in the FP2 sample is great, this value might indicate that in dilute Fe ultraphosphate samples, $Fe^{2+}$ ions can form $FeO_6$ octahedra. In ultraphosphate glasses of $x = 0.3$ (sample FP3) where more than six $O_T$ are available for each $Fe^{2+}$ only $FeO_5$ or strongly distorted $FeO_6$ polyhedra instead of well defined $FeO_6$ octahedra are formed. Thus, a reasonable fraction of the $O_T$ of this glass structure does not have close Me neighbours, a behaviour that is different from that for Mg and Zn ultraphosphate glasses (see figure 1) and unexpected from the structure of the related $FeP_4O_{11}$ crystal [40], where $N_{FeO} = \sim 6$.

The $T(r)$ functions of metaphosphate glasses with Me atoms of similar dimensions (Mg, Zn, Fe and Co) are shown in figure 5. The $T(r)$ data of the Mg, Zn and Co glasses are taken from [16]. The $T(r)$ function of the Zn metaphosphate glass shows a sharp Zn–O peak with $N_{ZnO} = \sim 4$ whereas the Mg–O peak at the same position is very asymmetric with a coordination number of ∼5.5. The coordination numbers $N_{FeO}$ and $N_{CoO}$ are ∼5, even though the distances $r_{FeO}$ and $r_{CoO}$ are greater than $r_{MgO}$. The $r_{FeO}$ and $r_{CoO}$ lengths agree with those of $MeO_6$ octahedra in $Fe_2P_4O_{12}$ [41] and $Co_2P_4O_{12}$ [47] crystals, respectively. The competition with the $Fe^{3+}$ cations is identified as the origin for the smaller coordination number found for the $Fe^{2+}$ cations. The origin for $N_{CoO} = \sim 5$ is not clear.

## 5. Conclusions

The use of high energy photons from a synchrotron in XRD investigations of $(FeO)_x(P_2O_5)_{1-x}$ glasses ($x = 0.2, 0.3, 0.4, 0.5$) with contaminations of 5–18% Fe(III) yield correlation functions with well resolved Fe–O peaks at 0.21 nm between the P–O and O–O peaks at 0.155 and 0.252 nm. Both latter peaks correspond to distances in the $PO_4$ tetrahedra. Constant P–O coordination numbers of $4.0 \pm 0.1$ as expected for tetrahedra demonstrate the reliability of the scattering data.

The oxygen coordination of the small Fe(III) fraction was set to six with Fe–O distances of 0.200 nm. Mean Fe(II)–O coordination numbers of ∼5 with distances of ∼0.210 nm are extracted from fitting the Fe–O peaks. These values are almost independent of the FeO content. With constant $N_{FeO}$ of five for the Fe(II) sites the behaviour of this metal–oxygen coordination is different from that of related crystal structures with $FeO_6$ octahedra and from that of Zn and Mg ultraphosphate glasses which show effects of a dependence of $N_{MeO}$ on the ratio of terminal oxygen per Me atoms. The explanation for the existence of $FeO_5$ (or strongly distorted $FeO_6$) polyhedra for the Fe(II) sites is given with specifics of a system with mixed oxide effects where the two fractions of $Fe^{2+}$ and $Fe^{3+}$ are assumed to be in competition. Thus, the behaviour of the Fe(II) environments cannot be interpreted in the sense of binary Fe(II) phosphate glasses.

## Acknowledgments

The authors from UMR acknowledge the donors of The Petroleum Research Fund, administered by the American Chemical Society, for support of this research.

## References

[1] Sales B C and Boatner L A 1984 *Science* **226** 45
[2] Sales B C and Boatner L A 1986 *J. Non-Cryst. Solids* **79** 83
[3] Sales B C, Abraham M M, Bates J B and Boatner L A 1985 *J. Non-Cryst. Solids* **71** 103
[4] Sales B C, Ramsey R S, Bates J B and Boatner L A 1986 *J. Non-Cryst. Solids* **87** 137
[5] Greaves G N, Gurman S J, Gladden L F, Spence C A, Cox P, Sales B C, Boatner L A and Jenkins R N 1988 *Phil. Mag.* B **58** 271
[6] Musinu A, Piccaluga G and Pinna G 1990 *J. Non-Cryst. Solids* **122** 52
[7] Yu X, Day D E, Long G J and Brow R K 1997 *J. Non-Cryst. Solids* **215** 21
[8] Marasinghe G K, Karabulut M, Ray C S, Day D E, Shumsky M G, Yelon W B, Booth C H, Allen P G and Shuh D K 1997 *J. Non-Cryst. Solids* **222** 144
[9] Karabulut M, Marasinghe G K, Ray C S, Waddill G D, Day D E, Badyal Y S, Saboungi M-L, Shastri S and Haeffner D 2000 *J. Appl. Phys.* **87** 2185
[10] Karabulut M, Marasinghe G K, Ray C S, Day D E, Waddill G D, Booth C H, Allen P G, Bucher J J, Caulder D L and Shuh D K 2002 *J. Non-Cryst. Solids* **306** 182
[11] Brow R K 2000 *J. Non-Cryst. Solids* **263/264** 1
[12] Hudgens J J and Martin S W 1993 *J. Am. Ceram. Soc.* **76** 1691
[13] Karabulut M, Metwalli E, Day D E and Brow R K 2003 *J. Non-Cryst. Solids* at press
[14] Hoppe U, Walter G, Kranold R, Stachel D and Barz A 1995 *J. Non-Cryst. Solids* **192/193** 28
[15] Hoppe U, Walter G, Stachel D, Barz A and Hannon A C 1997 *Z. Naturf.* a **52** 259
[16] Hoppe U, Kranold R, Barz A, Stachel D, Neuefeind J and Keen D K 2001 *J. Non-Cryst. Solids* **293–295** 158
[17] Suzuya K, Price D L, Loong C-K and Kohara S 1999 *J. Phys. Chem. Solids* **60** 1457
[18] Walter G, Vogel J, Hoppe U and Hartmann P 2003 *J. Non-Cryst. Solids* **320** 210
[19] Hoppe U 1996 *J. Non-Cryst. Solids* **195** 138
[20] Hoppe U, Walter G, Carl G, Neuefeind J and Hannon A C 2003 *J. Non-Cryst. Solids* at press
[21] Hoppe U, Metwalli E, Brow R K and Neuefeind J 2002 *J. Non-Cryst. Solids* **297** 263
[22] Karabulut M, Marasinghe G K, Metwalli E, Wittenauer A K and Brow R K 2002 *Phys. Rev.* B **65** 104206
[23] Brow R K, Click C A and Alam T M 2000 *J. Non-Cryst. Solids* **274** 9

[24] Hoppe U, Ilieva D and Neuefeind J 2002 *Z. Naturf.* a **57** 709
[25] Huheey J E 1983 *Principles of Structure and Reactivity* (*Inorganic Chemistry* 3rd edn) (New York: Harper and Row)
[26] Rossat-Mignod J 1987 *Methods of Experimental Physics* vol 23: *Neutron Scattering* part C ed K Sköld and D L Price (New York: Academic) p 97
[27] Poulsen H F, Neuefeind J, Neumann H-B, Schneider J R and Zeidler M D 1995 *J. Non-Cryst. Solids* **188** 63
[28] Waasmeier D and Kirfel A 1995 *Acta Crystallogr.* A **51** 416
[29] Maslen E N, Fox A G and O'Kiefe M A 1992 *International Tables for Crystallography* vol C, ed A J C Wilson (Dordrecht: Kluwer) p 476
[30] Hubbell J H, Veigele Wm J, Briggs E A, Brown R T, Cromer D T and Howerton R J 1975 *J. Phys. Chem. Ref. Data* **4** 471
[31] Faber T E and Ziman J M 1965 *Phil. Mag.* **11** 153
[32] Waseda Y 1980 *The Structure of Non-Crystalline Materials* (New York: McGraw-Hill) p 11
[33] Lorch E A 1969 *J. Phys. C: Solid State Phys.* **2** 229
[34] Warren B E 1969 *X-Ray Diffraction* (Reading, MA: Addison-Wesley) pp 135–42
[35] Mozzi R L and Warren B E 1969 *J. Appl. Crystallogr.* **2** 164
[36] Marquardt D 1963 *SIAM J. Appl. Math.* **11** 431
[37] Suzuki K and Ueno M 1985 *J. Physique Colloq. (Paris)* C 8 **46** 261
[38] Hoppe U, Walter G, Kranold R and Stachel D 2000 *J. Non-Cryst. Solids* **263/264** 29
[39] Elbouaanani L K, Malaman B and Gerardin R 1999 *J. Solid State Chem.* **148** 455
[40] Weil M and Glaum R 1998 *Eur. J. Solid State Inorg. Chem.* **35** 495
[41] Nord A G, Ericsson T and Werner P E 1990 *Z. Kristallogr.* **192** 83
[42] Stefanidis T and Nord A G 1982 *Z. Kristallogr.* **159** 255
[43] Kostiner E and Rea J R 1974 *Inorg. Chem.* **13** 2876
[44] Van Wazer J R 1958 *Phosphorus and its Compounds* vol 1 (New York: Interscience)
[45] Ijjaali M, Venturini G, Gerardin R, Malaman B and Gleitzer C 1991 *Eur. J. Solid State Inorg. Chem.* **28** 983
[46] Huang C and Cormack A N 1992 *J. Mater. Chem.* **2** 281
[47] Nord A G 1982 *Cryst. Struct. Commun.* **11** 1467